1. Supplementary Material

1.1. Transition from configurational space exploration to localisation

As the annealing temperature decreses, the chance of a configuration with high energy being accepted decreases. The evolution of the values taken by the parameters ϕ_1, θ_1, ϕ_3 and θ_3 clearly exhibited this trend. A plot of the values taken by ϕ_1 *versus* those of θ_1 at high temperatures ($T = 2.0$, Fig. 1A) shows a uniform distribution. At this temperature, the system explored the energy landscape, and thus the values taken by the parameters randomly span their whole variation ranges. A similar plot at a lower temperature ($T = 0.17$, Fig. 1B), shows that the parameter values are now somewhat confined, reflecting the localisation of the system in configurational space. Finally, at the lowest temperatures ($T = 0.01$), the system is stranded in the global minimum, and the parameter values are completely localised (Fig. 1C).

Parameter localisation was also observed by looking at the histograms of the values taken by each parameter *in accepted configurations* as the temperature decreases. At high temperatures ($T = 2.0$), the accepted configurations have parameters randomly distributed over their variation ranges. At lower temperatures ($T = 0.17$), the values taken by the parameters in accepted configurations have localised distributions. For even lower temperatures ($T = 0.01$, data not shown) a total localisation of the parameters at the configuration with minimum energy occurs.

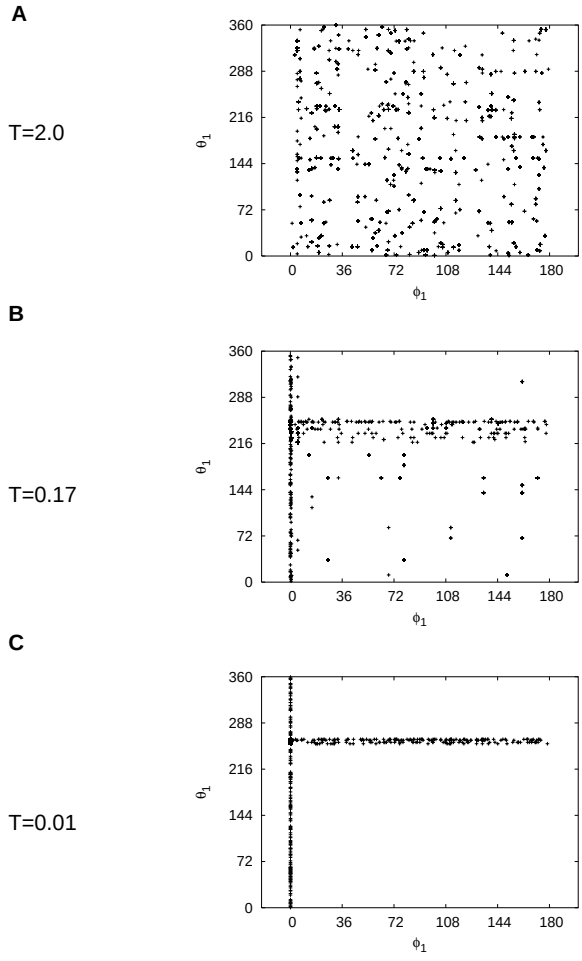

Fig. 1. Demonstration of parameter localisation. Plots of the values taken by ϕ_1 *versus* those of θ_1 at simulated annealing temperatures of (A) 2.0, (B) 0.17, and (C) 0.01, for a single run in the S9-X family of simulations.

1.2. Stability of the reconstruction process

The robustness of the reconstruction method in retrieving the original parameters was evaluated by applying different levels of noise to the simulated scattering data. Two additional simulated SAXS datasets, with noise levels 20 and 40 times larger than those of SAXS9, were produced ($SAXS9_{20}$ and $SAXS9_{40}$, Fig. 2B). Families of runs, using these SAXS datasets, either alone (S9-X-20 and S9-X-40) or in combination with the SV9 and FRET9 datasets (S9-HX-20 and S9-HXF-20), were performed. For

both S9-X-20 and S9-X-40, the original parameters were retrieved in all the runs performed (Table 3, Fig. 2). As expected, not only the difference between retrieved and original parameters (resulting in higher F-values) but also the parameter uncertainties augmented with increasing noise levels. As seen before, the inclusion of more datasets improved the reconstruction process. When the $SAXS9_{20}$, SV9 and FRET9 datasets were combined, the F-value decreased and the uncertainties in the parameters were reduced, with respect to using only the $SAXS_{20}$ dataset (S9-HXF-20, Table 3, Fig. 2, solid line). Even with large noise levels, the reconstruction process was successful in retrieving the *in silico* structures of blg9 and blg14 (see superpositions of *in silico* and reconstructed structures in Fig. 6B-C). This demonstrates the robustness of the method with respect to the introduction of high levels of noise in the datasets.

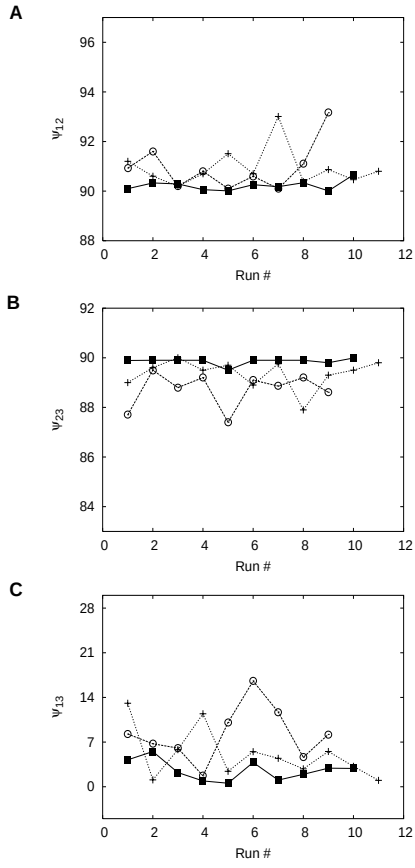

Fig. 2. Final results for simulations for blg9 with different noise levels. (A)-(C) Angles ψ_{12}, ψ_{23} and ψ_{13} for S9-X-20 (dotted line, crosses), S9-X-40 (dashed line, open circles), and S9-HXF-20 (solid line, filled boxes).

1.3. Reconstruction of the X-synapse

The low-resolution structure of the complex formed by four Tn3 resolvase subunits and two DNA fragments (X-synapse) was previously deduced from experimental small angle neutron and x-ray scattering data (Nöllmann *et al.*, 2004).

By using the computer program developed in this paper, we have reconstructed the low-resolution structure of this protein-DNA complex from the same SAXS and SANS datasets (datasets SAXS and SANS43, Figs. 3A and B, respectively). The SAXS dataset was obtained by measuring the SAXS intensity profile from an homogeneous

solution of concentrated X-synapse with four protein subunits and two 36 bp DNA fragments. The SANS43 dataset was obtained by measuring the SANS profile of a solution containing purified X-synapse with four protein subunits and two 50 bp DNA fragments at 43% v/v D_2O concentration.

1gdt is the co-crystal structure of the $\gamma\delta$ resolvase-DNA complex obtained by crystallographic methods (Yang & Steitz, 1995), and contains two protein subunits bound to a 36 bp DNA fragment. The reconstruction of the structure of the X-synapse from the SAXS dataset was performed by employing two 1gdt subunits (Nöllmann *et al.*, 2004). 1gdt50 was built using protein and DNA coordinates from 1gdt, and the DNA was extended by adding two 7 bp B-DNA fragments to its ends. The structure of the X-synapse was also reconstructed from the SANS43 dataset by using two 1gdt50 subunits. The parameters used for the reconstruction of the X-synapse structure in this paper (d and ϕ) were the same as those used in a previous study (Nöllmann *et al.*, 2004).

At least 10 reconstructions were performed for each dataset. For the SAXS dataset reconstruction, the restoration process was stable and converged in all runs to the same final parameters, namely $d = 60 \pm 3\mathring{A}$ and $\phi = 22 \pm 10^o$. The SANS43 reconstruction process produced restorations with a stable value of $d = 57 \pm 6$ Åand a value of ϕ that varied from 0 to 110^o. This ambiguity in the value of ϕ was noted before, and arises from the insensitivity of χ^2 to the variation in the angular parameter ϕ (Nöllmann *et al.*, 2004). The scattering profiles simulated from these reconstructions fit properly the experimental SAXS and SANS43 datasets (Fig. 3A and B) with χ^2-values similar to those obtained in a previous study (Nöllmann *et al.*, 2004).

The final parameters and the shape of the corresponding structural models of the X-synapse obtained from the SAXS and SANS43 datasets (Figs. 3C and D) agree well with those presented already found (Nöllmann *et al.*, 2004) (Fig. 3E).

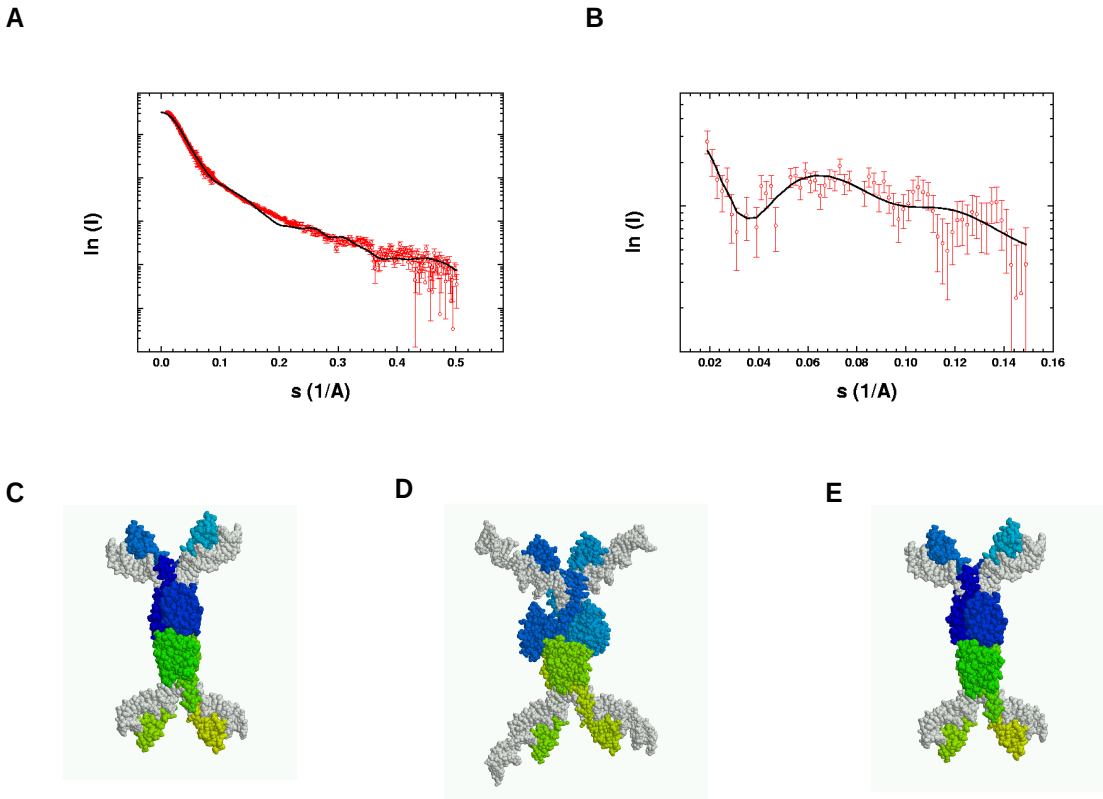

Fig. 3. Small angle scattering experimental data (*open circles*) with error bars (*vertical bars*) and best fits obtained by the final models obtained from the reconstructions of the (A) SAXS and the (B) SANS43 datasets (*solid lines*). The χ^2 of the fit for the SAXS dataset is 3.6, whereas that for the SANS43 dataset is $\chi^2 = 0.9$. Bottom panels show the final models for the X-synapse solution structure obtained from the reconstruction of (C) the SAXS dataset, (D) the SANS43 dataset, and (E) the final model proposed in (Nöllmann *et al.*, 2004).

References

Nöllmann, M., He, J., Byron, O. & Stark, W. M. (2004). *Mol. Cell*, **16**, 127–137.
Yang, W. & Steitz, T. A. (1995). *Cell*, **82**, 193–207.